DESY–12–089
June 2012

Measurement of isolated photons accompanied by jets in deep inelastic *ep* scattering

ZEUS Collaboration

Abstract

The production of isolated high-energy photons accompanied by jets has been measured in deep inelastic *ep* scattering with the ZEUS detector at HERA, using an integrated luminosity of $326\,\mathrm{pb}^{-1}$. Measurements were made for exchanged photon virtualities, Q^2, in the range 10 to $350\,\mathrm{GeV}^2$. The photons were measured in the transverse-energy and pseudorapidity ranges $4 < E_T^{\gamma} < 15$ GeV and $-0.7 < \eta^{\gamma} < 0.9$, and the jets were measured in the transverse-energy and pseudorapidity ranges $2.5 < E_T^{\mathrm{jet}} < 35$ GeV and $-1.5 < \eta^{\mathrm{jet}} < 1.8$. Differential cross sections are presented as functions of these quantities. Perturbative QCD predictions give a reasonable description of the shape of the measured cross sections over most of the kinematic range, but the absolute normalisation is typically in disagreement by 20-30%.

The ZEUS Collaboration

H. Abramowicz[45,ai], I. Abt[35], L. Adamczyk[13], M. Adamus[54], R. Aggarwal[7,c], S. Antonelli[4], P. Antonioli[3], A. Antonov[33], M. Arneodo[50], O. Arslan[5], V. Aushev[26,27,aa], Y. Aushev,[27,aa,ab], O. Bachynska[15], A. Bamberger[19], A.N. Barakbaev[25], G. Barbagli[17], G. Bari[3], F. Barreiro[30], N. Bartosik[15], D. Bartsch[5], M. Basile[4], O. Behnke[15], J. Behr[15], U. Behrens[15], L. Bellagamba[3], A. Bertolin[39], S. Bhadra[57], M. Bindi[4], C. Blohm[15], V. Bokhonov[26,aa], T. Bołd[13], K. Bondarenko[27], E.G. Boos[25], K. Borras[15], D. Boscherini[3], D. Bot[15], I. Brock[5], E. Brownson[56], R. Brugnera[40], N. Brümmer[37], A. Bruni[3], G. Bruni[3], B. Brzozowska[53], P.J. Bussey[20], B. Bylsma[37], A. Caldwell[35], M. Capua[8], R. Carlin[40], C.D. Catterall[57], S. Chekanov[1], J. Chwastowski[12,e], J. Ciborowski[53,am], R. Ciesielski[15,h], L. Cifarelli[4], F. Cindolo[3], A. Contin[4], A.M. Cooper-Sarkar[38], N. Coppola[15,i], M. Corradi[3], F. Corriveau[31], M. Costa[49], G. D'Agostini[43], F. Dal Corso[39], J. del Peso[30], R.K. Dementiev[34], S. De Pasquale[4,a], M. Derrick[1], R.C.E. Devenish[38], D. Dobur[19,t], B.A. Dolgoshein [33,†], G. Dolinska[27], A.T. Doyle[20], V. Drugakov[16], L.S. Durkin[37], S. Dusini[39], Y. Eisenberg[55], P.F. Ermolov [34,†], A. Eskreys [12,†], S. Fang[15,j], S. Fazio[8], J. Ferrando[20], M.I. Ferrero[49], J. Figiel[12], M. Forrest[20,w], B. Foster[38,ae], G. Gach[13], A. Galas[12], E. Gallo[17], A. Garfagnini[40], A. Geiser[15], I. Gialas[21,x], A. Gizhko[27,ac], L.K. Gladilin[34,ad], D. Gladkov[33], C. Glasman[30], O. Gogota[27], Yu.A. Golubkov[34], P. Göttlicher[15,k], I. Grabowska-Bołd[13], J. Grebenyuk[15], I. Gregor[15], G. Grigorescu[36], G. Grzelak[53], O. Gueta[45], M. Guzik[13], C. Gwenlan[38,af], T. Haas[15], W. Hain[15], R. Hamatsu[48], J.C. Hart[44], H. Hartmann[5], G. Hartner[57], E. Hilger[5], D. Hochman[55], R. Hori[47], A. Hüttmann[15], Z.A. Ibrahim[10], Y. Iga[42], R. Ingbir[45], M. Ishitsuka[46], H.-P. Jakob[5], F. Januschek[15], T.W. Jones[52], M. Jüngst[5], I. Kadenko[27], B. Kahle[15], S. Kananov[45], T. Kanno[46], U. Karshon[55], F. Karstens[19,u], I.I. Katkov[15,l], M. Kaur[7], P. Kaur[7,c], A. Keramidas[36], L.A. Khein[34], J.Y. Kim[9], D. Kisielewska[13], S. Kitamura[48,ak], R. Klanner[22], U. Klein[15,m], E. Koffeman[36], N. Kondrashova[27,ac], O. Kononenko[27], P. Kooijman[36], Ie. Korol[27], I.A. Korzhavina[34,ad], A. Kotański[14,f], U. Kötz[15], H. Kowalski[15], O. Kuprash[15], M. Kuze[46], A. Lee[37], B.B. Levchenko[34], A. Levy[45], V. Libov[15], S. Limentani[40], T.Y. Ling[37], M. Lisovyi[15], E. Lobodzinska[15], W. Lohmann[16], B. Löhr[15], E. Lohrmann[22], K.R. Long[23], A. Longhin[39,ag], D. Lontkovskyi[15], O.Yu. Lukina[34], J. Maeda[46,aj], S. Magill[1], I. Makarenko[15], J. Malka[15], R. Mankel[15], A. Margotti[3], G. Marini[43], J.F. Martin[51], A. Mastroberardino[8], M.C.K. Mattingly[2], I.-A. Melzer-Pellmann[15], S. Mergelmeyer[5], S. Miglioranzi[15,n], F. Mohamad Idris[10], V. Monaco[49], A. Montanari[15], J.D. Morris[6,b], K. Mujkic[15,o], B. Musgrave[1], K. Nagano[24], T. Namsoo[15,p], R. Nania[3], A. Nigro[43], Y. Ning[11], T. Nobe[46], D. Notz[15], R.J. Nowak[53], A.E. Nuncio-Quiroz[5], B.Y. Oh[41], N. Okazaki[47], K. Olkiewicz[12], Yu. Onishchuk[27], K. Papageorgiu[21], A. Parenti[15], E. Paul[5], J.M. Pawlak[53], B. Pawlik[12], P. G. Pelfer[18], A. Pellegrino[36], W. Perlański[53,an], H. Perrey[15], K. Piotrzkowski[29], P. Pluciński[54,ao], N.S. Pokrovskiy[25], A. Polini[3], A.S. Proskuryakov[34], M. Przybycień[13], A. Raval[15], D.D. Reeder[56], B. Reisert[35], Z. Ren[11], J. Repond[1], Y.D. Ri[48,al], A. Robertson[38], P. Roloff[15,n], I. Rubinsky[15], M. Ruspa[50], R. Sacchi[49], U. Samson[5], G. Sartorelli[4], A.A. Savin[56], D.H. Saxon[20], M. Schioppa[8], S. Schlenstedt[16], P. Schleper[22], W.B. Schmidke[35], U. Schneekloth[15], V. Schönberg[5], T. Schörner-Sadenius[15], J. Schwartz[31], F. Sciulli[11], L.M. Shcheglova[34], R. Shehzadi[5], S. Shimizu[47,n], I. Singh[7,c], I.O. Skillicorn[20], W. Słomiński[14,g], W.H. Smith[56], V. Sola[22], A. Solano[49], D. Son[28], V. Sosnovtsev[33], A. Spiridonov[15,q], H. Stadie[22], L. Stanco[39], N. Stefaniuk[27], A. Stern[45], T.P. Stewart[51], A. Stifutkin[33], P. Stopa[12], S. Suchkov[33], G. Susinno[8], L. Suszycki[13], J. Sztuk-Dambietz[22], D. Szuba[22], J. Szuba[15,r], A.D. Tapper[23], E. Tassi[8,d], J. Terrón[30], T. Theedt[15], H. Tiecke[36], K. Tokushuku[24,y],

J. Tomaszewska[15,s], V. Trusov[27], T. Tsurugai[32], M. Turcato[22], O. Turkot[27,ac], T. Tymieniecka[54,ap], M. Vázquez[36,n], A. Verbytskyi[15], O. Viazlo[27], N.N. Vlasov[19,v], R. Walczak[38], W.A.T. Wan Abdullah[10], J.J. Whitmore[41,ah], K. Wichmann[15], L. Wiggers[36], M. Wing[52], M. Wlasenko[5], G. Wolf[15], H. Wolfe[56], K. Wrona[15], A.G. Yagües-Molina[15], S. Yamada[24], Y. Yamazaki[24,z], R. Yoshida[1], C. Youngman[15], O. Zabiegalov[27,ac], A.F. Żarnecki[53], L. Zawiejski[12], O. Zenaiev[15], W. Zeuner[15,n], B.O. Zhautykov[25], N. Zhmak[26,aa], A. Zichichi[4], Z. Zolkapli[10], D.S. Zotkin[34]

[1] *Argonne National Laboratory, Argonne, Illinois 60439-4815, USA* [A]
[2] *Andrews University, Berrien Springs, Michigan 49104-0380, USA*
[3] *INFN Bologna, Bologna, Italy* [B]
[4] *University and INFN Bologna, Bologna, Italy* [B]
[5] *Physikalisches Institut der Universität Bonn, Bonn, Germany* [C]
[6] *H.H. Wills Physics Laboratory, University of Bristol, Bristol, United Kingdom* [D]
[7] *Panjab University, Department of Physics, Chandigarh, India*
[8] *Calabria University, Physics Department and INFN, Cosenza, Italy* [B]
[9] *Institute for Universe and Elementary Particles, Chonnam National University, Kwangju, South Korea*
[10] *Jabatan Fizik, Universiti Malaya, 50603 Kuala Lumpur, Malaysia* [E]
[11] *Nevis Laboratories, Columbia University, Irvington on Hudson, New York 10027, USA* [F]
[12] *The Henryk Niewodniczanski Institute of Nuclear Physics, Polish Academy of Sciences, Krakow, Poland* [G]
[13] *AGH-University of Science and Technology, Faculty of Physics and Applied Computer Science, Krakow, Poland* [H]
[14] *Department of Physics, Jagellonian University, Cracow, Poland*
[15] *Deutsches Elektronen-Synchrotron DESY, Hamburg, Germany*
[16] *Deutsches Elektronen-Synchrotron DESY, Zeuthen, Germany*
[17] *INFN Florence, Florence, Italy* [B]
[18] *University and INFN Florence, Florence, Italy* [B]
[19] *Fakultät für Physik der Universität Freiburg i.Br., Freiburg i.Br., Germany*
[20] *School of Physics and Astronomy, University of Glasgow, Glasgow, United Kingdom* [D]
[21] *Department of Engineering in Management and Finance, Univ. of the Aegean, Chios, Greece*
[22] *Hamburg University, Institute of Experimental Physics, Hamburg, Germany* [I]
[23] *Imperial College London, High Energy Nuclear Physics Group, London, United Kingdom* [D]
[24] *Institute of Particle and Nuclear Studies, KEK, Tsukuba, Japan* [J]
[25] *Institute of Physics and Technology of Ministry of Education and Science of Kazakhstan, Almaty, Kazakhstan*
[26] *Institute for Nuclear Research, National Academy of Sciences, Kyiv, Ukraine*
[27] *Department of Nuclear Physics, National Taras Shevchenko University of Kyiv, Kyiv, Ukraine*
[28] *Kyungpook National University, Center for High Energy Physics, Daegu, South Korea* [K]
[29] *Institut de Physique Nucléaire, Université Catholique de Louvain, Louvain-la-Neuve, Belgium* [L]
[30] *Departamento de Física Teórica, Universidad Autónoma de Madrid, Madrid, Spain* [M]
[31] *Department of Physics, McGill University, Montréal, Québec, Canada H3A 2T8* [N]
[32] *Meiji Gakuin University, Faculty of General Education, Yokohama, Japan* [J]
[33] *Moscow Engineering Physics Institute, Moscow, Russia* [O]

[34] *Lomonosov Moscow State University, Skobeltsyn Institute of Nuclear Physics, Moscow, Russia* [P]
[35] *Max-Planck-Institut für Physik, München, Germany*
[36] *NIKHEF and University of Amsterdam, Amsterdam, Netherlands* [Q]
[37] *Physics Department, Ohio State University, Columbus, Ohio 43210, USA* [A]
[38] *Department of Physics, University of Oxford, Oxford, United Kingdom* [D]
[39] *INFN Padova, Padova, Italy* [B]
[40] *Dipartimento di Fisica dell' Università and INFN, Padova, Italy* [B]
[41] *Department of Physics, Pennsylvania State University, University Park, Pennsylvania 16802, USA* [F]
[42] *Polytechnic University, Tokyo, Japan* [J]
[43] *Dipartimento di Fisica, Università 'La Sapienza' and INFN, Rome, Italy* [B]
[44] *Rutherford Appleton Laboratory, Chilton, Didcot, Oxon, United Kingdom* [D]
[45] *Raymond and Beverly Sackler Faculty of Exact Sciences, School of Physics, Tel Aviv University, Tel Aviv, Israel* [R]
[46] *Department of Physics, Tokyo Institute of Technology, Tokyo, Japan* [J]
[47] *Department of Physics, University of Tokyo, Tokyo, Japan* [J]
[48] *Tokyo Metropolitan University, Department of Physics, Tokyo, Japan* [J]
[49] *Università di Torino and INFN, Torino, Italy* [B]
[50] *Università del Piemonte Orientale, Novara, and INFN, Torino, Italy* [B]
[51] *Department of Physics, University of Toronto, Toronto, Ontario, Canada M5S 1A7* [N]
[52] *Physics and Astronomy Department, University College London, London, United Kingdom* [D]
[53] *Faculty of Physics, University of Warsaw, Warsaw, Poland*
[54] *National Centre for Nuclear Research, Warsaw, Poland*
[55] *Department of Particle Physics and Astrophysics, Weizmann Institute, Rehovot, Israel*
[56] *Department of Physics, University of Wisconsin, Madison, Wisconsin 53706, USA* [A]
[57] *Department of Physics, York University, Ontario, Canada M3J 1P3* [N]

[A] supported by the US Department of Energy
[B] supported by the Italian National Institute for Nuclear Physics (INFN)
[C] supported by the German Federal Ministry for Education and Research (BMBF), under contract No. 05 H09PDF
[D] supported by the Science and Technology Facilities Council, UK
[E] supported by an FRGS grant from the Malaysian government
[F] supported by the US National Science Foundation. Any opinion, findings and conclusions or recommendations expressed in this material are those of the authors and do not necessarily reflect the views of the National Science Foundation.
[G] supported by the Polish Ministry of Science and Higher Education as a scientific project No. DPN/N188/DESY/2009
[H] supported by the Polish Ministry of Science and Higher Education and its grants for Scientific Research
[I] supported by the German Federal Ministry for Education and Research (BMBF), under contract No. 05h09GUF, and the SFB 676 of the Deutsche Forschungsgemeinschaft (DFG)
[J] supported by the Japanese Ministry of Education, Culture, Sports, Science and Technology (MEXT) and its grants for Scientific Research
[K] supported by the Korean Ministry of Education and Korea Science and Engineering Foundation
[L] supported by FNRS and its associated funds (IISN and FRIA) and by an Inter-University Attraction Poles Programme subsidised by the Belgian Federal Science Policy Office
[M] supported by the Spanish Ministry of Education and Science through funds provided by CICYT
[N] supported by the Natural Sciences and Engineering Research Council of Canada (NSERC)
[O] partially supported by the German Federal Ministry for Education and Research (BMBF)
[P] supported by RF Presidential grant N 4142.2010.2 for Leading Scientific Schools, by the Russian Ministry of Education and Science through its grant for Scientific Research on High Energy Physics and under contract No.02.740.11.0244
[Q] supported by the Netherlands Foundation for Research on Matter (FOM)
[R] supported by the Israel Science Foundation

[a] now at University of Salerno, Italy
[b] now at Queen Mary University of London, United Kingdom
[c] also funded by Max Planck Institute for Physics, Munich, Germany
[d] also Senior Alexander von Humboldt Research Fellow at Hamburg University, Institute of Experimental Physics, Hamburg, Germany
[e] also at Cracow University of Technology, Faculty of Physics, Mathemathics and Applied Computer Science, Poland
[f] supported by the research grant No. 1 P03B 04529 (2005-2008)
[g] supported by the Polish National Science Centre, project No. DEC-2011/01/BST2/03643
[h] now at Rockefeller University, New York, NY 10065, USA
[i] now at DESY group FS-CFEL-1
[j] now at Institute of High Energy Physics, Beijing, China
[k] now at DESY group FEB, Hamburg, Germany
[l] also at Moscow State University, Russia
[m] now at University of Liverpool, United Kingdom
[n] now at CERN, Geneva, Switzerland
[o] also affiliated with Universtiy College London, UK
[p] now at Goldman Sachs, London, UK
[q] also at Institute of Theoretical and Experimental Physics, Moscow, Russia
[r] also at FPACS, AGH-UST, Cracow, Poland
[s] partially supported by Warsaw University, Poland
[t] now at Istituto Nucleare di Fisica Nazionale (INFN), Pisa, Italy
[u] now at Haase Energie Technik AG, Neumünster, Germany
[v] now at Department of Physics, University of Bonn, Germany
[w] now at Biodiversität und Klimaforschungszentrum (BiK-F), Frankfurt, Germany
[x] also affiliated with DESY, Germany
[y] also at University of Tokyo, Japan
[z] now at Kobe University, Japan
[†] deceased
[aa] supported by DESY, Germany
[ab] member of National Technical University of Ukraine, Kyiv Polytechnic Institute, Kyiv, Ukraine
[ac] member of National University of Kyiv - Mohyla Academy, Kyiv, Ukraine
[ad] partly supported by the Russian Foundation for Basic Research, grant 11-02-91345-DFG_a
[ae] Alexander von Humboldt Professor; also at DESY and University of Oxford
[af] STFC Advanced Fellow
[ag] now at LNF, Frascati, Italy
[ah] This material was based on work supported by the National Science Foundation, while working at the Foundation.
[ai] also at Max Planck Institute for Physics, Munich, Germany, External Scientific Member
[aj] now at Tokyo Metropolitan University, Japan
[ak] now at Nihon Institute of Medical Science, Japan

[al] now at Osaka University, Osaka, Japan
[am] also at Łódź University, Poland
[an] member of Łódź University, Poland
[ao] now at Department of Physics, Stockholm University, Stockholm, Sweden
[ap] also at Cardinal Stefan Wyszyński University, Warsaw, Poland

1 Introduction

Events in which an isolated high-energy photon is observed provide a direct probe of the underlying partonic process in high-energy collisions involving hadrons, since the emission of such photons is unaffected by parton hadronisation. Processes of this kind have been studied in a number of fixed-target and hadron-collider experiments [1]. In ep collisions at HERA, the ZEUS and H1 collaborations have previously reported the production of isolated photons in photoproduction [2–6], in which the exchanged photon is quasi-real, and also in deep inelastic scattering (DIS) [7–9], where the virtuality Q^2 of the exchanged virtual photon is greater than 1 GeV^2. The analysis presented here follows a recent ZEUS inclusive measurement [9] of isolated photons in DIS.

Figure 1 shows the lowest-order tree-level diagrams for high-energy photon production in DIS. Photons radiated by an incoming or outgoing quark are called "prompt"; an additional class of photons comprises those radiated from the incoming or outgoing lepton. In this paper, the inclusive photon measurements in DIS by ZEUS are extended to include the requirement of a hadronic jet. By increasing the ratio of the prompt photon contribution relative to the lepton-radiated contributions, this measurement provides an improved test of perturbative QCD (pQCD) in a kinematic region with two hard scales, which are given by Q and by $p_T^{\rm jet}$, the transverse momentum of the jet or, equivalently, the momentum transfer in the QCD scatter. In particular, the fraction of prompt processes is increased, and a class of jetless non-pQCD processes is excluded in which a soft photon radiated within the proton undergoes a hard scatter off the incoming electron [10]. Compared to a previous ZEUS publication on this topic [7], the kinematic reach extends to lower values of Q^2 and to higher values of the photon transverse energy, E_T^γ, and the statistical precision is much improved owing to the availability of nearly three times the integrated luminosity.

Leading-logarithm parton-shower Monte Carlo (MC) and perturbative QCD predictions are compared to the measurements. The cross sections for isolated photon production in DIS have been calculated to order $O(\alpha^3\alpha_s)$ by Gehrmann-De Ridder *et al.* (GKS) [11–13]. A calculation based on the k_T factorisation approach has been made by Baranov *et al.* (BLZ) [14].

2 Experimental set-up

The measurements are based on a data sample corresponding to an integrated luminosity of $326 \pm 6\,\mathrm{pb}^{-1}$, taken during the years 2004 to 2007 with the ZEUS detector at HERA. During this period, HERA ran with an electron/positron beam energy of 27.5 GeV and a

proton beam energy of 920 GeV. The sample is a sum of $138 \pm 2\,\mathrm{pb}^{-1}$ of e^+p data and $188 \pm 3\,\mathrm{pb}^{-1}$ of e^-p data[1].

A detailed description of the ZEUS detector can be found elsewhere [15]. Charged particles were tracked in the central tracking detector (CTD) [16] and a silicon micro vertex detector (MVD) [17] which operated in a magnetic field of 1.43 T provided by a thin superconducting solenoid. The high-resolution uranium–scintillator calorimeter (CAL) [18] consisted of three parts: the forward (FCAL), the barrel (BCAL) and the rear (RCAL) calorimeters. The BCAL covered the pseudorapidity range –0.74 to 1.01 as seen from the nominal interaction point. The FCAL and RCAL extended the range to –3.5 to 4.0. The smallest subdivision of the CAL was called a cell. The barrel electromagnetic calorimeter (BEMC) cells had a pointing geometry aimed at the nominal interaction point, with a cross section approximately $5 \times 20\,\mathrm{cm}^2$, with the finer granularity in the Z-direction[2]. This fine granularity allows the use of shower-shape distributions to distinguish isolated photons from the products of neutral meson decays such as $\pi^0 \to \gamma\gamma$.

The luminosity was measured using the Bethe–Heitler reaction $ep \to e\gamma p$ by a luminosity detector which consisted of two independent systems: a lead–scintillator calorimeter [19] and a magnetic spectrometer [20].

3 Event selection and reconstruction

A three-level trigger system was used to select events online [15, 21, 22] by requiring well isolated electromagnetic deposits in the CAL.

Events were selected offline by requiring a scattered-electron candidate, identified using a neural network [23]. The candidates were required to have a polar angle in the range $\theta_e > 140^\circ$, in order to have a good measurement in the RCAL. To ensure a well understood acceptance, the impact point (X,Y) of the candidate on the surface of the RCAL was required to lie outside a rectangular region (± 14.8 cm in X and $[-14.6, +12.5]$ cm in Y) centred on the origin of coordinates. The energy of the candidate, E'_e, was required to be larger than 10 GeV. The kinematic quantities Q^2 and x were reconstructed from the scattered electron as $Q^2 = -(k - k')^2$ and $x = Q^2/(2P \cdot (k - k'))$, where k (k') is the four-momentum of the incoming (outgoing) lepton and P is the four-momentum of the incoming proton. The kinematic region $10 < Q^2 < 350\,\mathrm{GeV}^2$ was selected.

To reduce backgrounds from non-ep collisions, events were required to have a reconstructed vertex position, Z_{vtx}, within the range $|Z_{\mathrm{vtx}}| < 40$ cm and to have $35 < E - p_Z < 65$ GeV,

[1] Hereafter 'electron' refers to both electrons and positrons unless otherwise stated.

[2] The ZEUS coordinate system is a right-handed Cartesian system, with the Z axis pointing in the proton beam direction, referred to as the "forward direction", and the X axis pointing towards the centre of HERA. The coordinate origin is at the nominal interaction point.

where $E - p_Z = \sum_i E_i(1 - \cos\theta_i)$; E_i is the energy of the i-th CAL cell, θ_i is its polar angle and the sum runs over all cells [24]. The latter cut also removes events with large initial-state radiation and low-Q^2 (photoproduction) events.

Energy-flow objects (EFOs) [25] were constructed from calorimeter-cell clusters, associated with tracks when appropriate. Photon candidates were identified as trackless EFOs for which at least 90% of the reconstructed energy was measured in the BEMC. EFOs with wider electromagnetic showers than are typical for a single photon were accepted to allow evaluation of backgrounds. The reconstructed transverse energy of the photon candidate, E_T^γ, was required to lie within the range $4 < E_T^\gamma < 15\,\text{GeV}$ and the pseudorapidity, η^γ, had to satisfy $-0.7 < \eta^\gamma < 0.9$. The upper limit on the reconstructed transverse energy was selected to ensure that the shower shapes from the hadronic background and the photon signal remained distinguishable.

Each event was required to contain an electron, a photon candidate and at least one accompanying jet. Jet reconstruction was performed on all EFOs in the event, including the electron and photon candidates, using the k_T clustering algorithm [26] in the E-scheme in the longitudinally invariant inclusive mode [27] with the R parameter set to 1.0. The jets were required to have transverse energy, E_T^{jet}, above 2.5 GeV and to lie within the pseudorapidity, η^{jet}, range $-1.5 < \eta^{\text{jet}} < 1.8$. One of the jets found by this procedure corresponds to or includes the photon candidate. An additional accompanying jet was required; if more than one was found, that with the highest E_T^{jet} was used.

To reduce the background from photons and neutral mesons within jets, and from photons radiated from electrons or positrons, the photon candidate was required to be isolated from the reconstructed tracks and other hadronic activity. The isolation from tracks was achieved by demanding $\Delta R > 0.2$, where $\Delta R = \sqrt{(\Delta\phi)^2 + (\Delta\eta)^2}$ is the distance to the nearest reconstructed track with momentum greater than 250 MeV in the $\eta - \phi$ plane, where ϕ is the azimuthal angle. Isolation from other hadronic activity was imposed by requiring that the photon candidate possessed at least 90% of the total energy of the reconstructed jet of which it formed a part.

A total of 6167 events were selected at this stage; the sample was dominated by background events. The largest source of background came from neutral current DIS events in which the scattered electron was detected in the RCAL, and one or more neutral mesons such as π^0 and η, decaying to photons, produced a photon candidate in the BEMC.

4 Theory

Two theoretical predictions are compared to the measurements presented in this paper. In the approach of GKS [11–13], the contributions to the scattering cross section for $ep \to e\gamma X$

are calculated at order α^3, referred to here as LO, and $\alpha^3\alpha_s$, referred to here as NLO, in the electromagnetic and strong couplings. One of these contributions comes from the radiation of a photon from the quark line (called QQ photons; Fig. 1a,b) and a second from the radiation from the lepton line (called LL photons; Fig. 1c,d). In addition to QQ and LL photons, an interference term between photon emission from the lepton and quark lines, called LQ photons by GKS, is present. For the kinematic region considered here, where the outgoing photon is well separated from both outgoing electron and quark, the interference term gives only a 3% effect on the cross section. This effect is further reduced to $\approx 1\%$ when e^+p and e^-p data are combined as the LQ term changes sign when e^- is replaced by e^+. The QQ contribution includes photon emission at wide angles from the quark as well as the leading $q \to q\gamma$ fragmentation term.

The GKS predictions use HERAPDF1.0 parton distribution functions for the proton [28] and the BFG parton-photon fragmentation functions [29]. For their NLO calculation, the authors quote an overall theoretical uncertainty of $(+4.3\%, -5.2\%)$ on their integrated cross section, rising to approximately $\pm 10\%$ at large negative jet rapidities. The uncertainty due to the choice of proton parton distributions is typically much less than 5%. The k_T factorisation method used by BLZ [14] takes into account the photon radiation from the lepton as well as the quarks. Unintegrated proton parton densities are used. This procedure gives a quark-radiated contribution that is enhanced relative to the leading-order collinear approximations. The uncertainties of up to 20% in the calculation are due mainly to the procedure of selecting jets from the evolution cascade in the factorisation approach.

In evaluating their predictions for the present data, both sets of authors have incorporated the experimental selections and photon-isolation procedure at the parton level. Hadronisation corrections were evaluated (see Section 5) to enable the predictions to be compared to the experimental data which are corrected to the hadron level.

5 Monte Carlo event simulation

Monte Carlo event samples were generated to evaluate the detector acceptance and to provide signal and background distributions. The program Pythia 6.416 [30] was used to simulate prompt-photon emission for the study of the event-reconstruction efficiency. In Pythia, this process is simulated as a DIS process with additional photon radiation from the quark line to account for QQ photons. Radiation from the lepton is not simulated.

The LL photons radiated at large angles from the incoming or outgoing electron were simulated using the generator Djangoh 6 [31], an interface to the MC program Heracles 4.6.6 [32]; higher-order QCD effects were included using the colour dipole model of Ariadne 4.12 [33]. Hadronisation of the partonic final state was in each case performed

by JETSET 7.4 [34] using the Lund string model [35]. The small LQ contribution was neglected.

The main background to the QQ and LL photons came from photonic decays of neutral mesons produced in general DIS processes. This background was simulated using DJANGOH 6, within the same framework as the LL events. This provided a realistic spectrum of single and multiple mesons with well modelled kinematic distributions.

The generated MC events were passed through the ZEUS detector and trigger simulation programs based on GEANT 3.21 [36]. They were reconstructed and analysed by the same programs as the data.

Hadronisation corrections to the theory calculations were evaluated using PYTHIA and ARIADNE, and typically lowered the theoretical prediction by about 10% with typical uncertainties of a few percent. They were calculated by running the same jet algorithm and event selections on the generated partons and on the hadronised final state in the MC events.

6 Extraction of the photon signal

The event sample selected according to the criteria described in Section 3 was dominated by background; thus the photon signal was extracted statistically following the approach used in previous ZEUS analyses [2–4, 7, 9].

The photon signal was extracted from the background using the lateral width of the BEMC energy-cluster comprising the photon candidate. This was calculated as the variable $\langle \delta Z \rangle = \sum_i E_i |Z_i - Z_{\rm cluster}| \; / (w_{\rm cell} \sum_i E_i)$. Here, Z_i is the Z position of the centre of the i-th cell, $Z_{\rm cluster}$ is the centroid of the EFO cluster, $w_{\rm cell}$ is the width of the cell in the Z direction, and E_i is the energy recorded in the cell. The sum runs over all BEMC cells in the EFO.

The global distribution of $\langle \delta Z \rangle$ in the data and in the MC are shown in Fig. 2a. The MC distributions in LL and QQ have been corrected using a comparison between the shapes in $\langle \delta Z \rangle$ associated with the scattered electron in MC simulation of DIS and in real data. The $\langle \delta Z \rangle$ distribution exhibits a double-peaked structure with the first peak at ≈ 0.1, associated with the photon signal, and a second peak at ≈ 0.5, dominated by the $\pi^0 \to \gamma\gamma$ background.

As a check, an alternative method was applied in which the quantity $f_{\rm max}$ was employed instead of $\langle \delta Z \rangle$, where $f_{\rm max}$ is the fraction of the photon-candidate shower contained in the BEMC cell with the largest signal. The results (Fig. 2b) were consistent with the main analysis method and showed no significant systematic difference.

The number of isolated-photon events contributing to the data is illustrated in Fig. 2a. It is determined for each cross-section bin by a χ^2 fit to the $\langle \delta Z \rangle$ distribution in the range $0 < \langle \delta Z \rangle < 0.8$, using the LL and QQ signal and background MC distributions as described in Section 5. By treating the LL and QQ photons separately, account is taken of their differing hadronic activity (resulting in significantly different acceptances) and their differing (η, E_T) distributions (resulting in different bin migrations due to finite measuring precision).

In performing the fit, the theoretically well determined LL contribution was kept constant at its MC-predicted value and the other components were varied. Of the 6167 events selected, 2440 ± 60 correspond to the extracted signal (LL and QQ). The scale factor resulting from the global fit for the QQ photons in Fig. 2a was 1.6; this factor was used for all the plots comparing MC to data. The fitted global scale factor for the hadronic background was 1.0. In all cross-section bins, the χ^2/n.d.f. of the fits was 2.3 or smaller.

For a given observable Y, the production cross section was determined using

$$\frac{d\sigma}{dY} = \frac{\mathcal{A}_{\mathrm{QQ}} \cdot N(\gamma_{\mathrm{QQ}})}{\mathcal{L} \cdot \Delta Y} + \frac{d\sigma^{\mathrm{MC}}_{\mathrm{LL}}}{dY},$$

where $N(\gamma_{\mathrm{QQ}})$ is the number of QQ photons extracted from the fit, ΔY is the bin width, $\mathcal{L}$ is the total integrated luminosity, $\sigma^{\mathrm{MC}}_{\mathrm{LL}}$ is the predicted cross section for LL photons from DJANGOH, and $\mathcal{A}_{\mathrm{QQ}}$ is the acceptance correction for QQ photons. The value of $\mathcal{A}_{\mathrm{QQ}}$ was calculated using Monte Carlo from the ratio of the number of events generated to those reconstructed in a given bin. It varied between 1.0 and 1.5 from bin to bin. To improve the representation of the data, and hence the accuracy of the acceptance corrections, the Monte Carlo predictions were reweighted. This was done globally as a function of Q^2 and of η^γ, and bin-by-bin as a function of photon energy; the three reweighting factors were applied multiplicatively.

7 Systematic uncertainties

The significant sources of systematic uncertainty were taken into account as follows:

- the energy of the measured scattered electron was varied by its known scale uncertainty of $\pm 2\%$ [38], causing variations in the measured cross sections of up to $\pm 5\%$;
- the energy of the photon candidate was similarly varied by $\pm 2\%$, causing variations in the measured cross sections of up to $\pm 5\%$;

- the modelling of the jets, and in particular the energy scale, was first studied for jets with $E_T^{\rm jet} > 10$ GeV by selecting ZEUS DIS events having one jet of this type and no photon or other jets with $E_T^{\rm jet} > 10$ GeV. Using the scattered electron, and requiring transverse-momentum balance, a prediction was made for the transverse energy of the jet, which was compared to the values obtained in the data and in the MC events. In this way, an uncertainty on the energy scale of $\pm 1.5\%$ was established for these jets. For jets with $E_T^{\rm jet}$ in the range [2.5, 10] GeV, DIS events were selected containing one jet in this range and one jet with $E_T^{\rm jet} > 10$ GeV. Using the scattered electron and the well measured high-energy jet, again requiring transverse-momentum balance, a prediction was made of the lower jet $E_T^{\rm jet}$ value, which was compared to the values obtained in data and in MC. In this way, the uncertainty on the jet energy scale was evaluated as $\pm 4\%$ and $\pm 2.5\%$ in the energy ranges [2.5, 6] and [6, 10] GeV, respectively. The resulting systematic uncertainty on the cross section was typically around $\pm 2\%$, ranging to $\pm 10\%$ at the highest $E_T^{\rm jet}$ values.

Since the photon and jet energy scales were calibrated relative to that of the scattered electron, all three energy-scale uncertainties were treated as correlated. The three energy scales were simultaneously varied by the uncertainties described above, and the resulting change in the cross sections was taken as the overall systematic energy-scale uncertainty. Further systematic uncertainties were evaluated as follows:

- the dependence on the modelling of the hadronic background by ARIADNE was investigated by varying the upper limit for the $\langle \delta Z \rangle$ fit in the range $[0.6, 1.0]$, giving variations that were typically $\pm 5\%$ increasing to $+12\%$ and -14% in the most forward η^γ and highest-x bins respectively;

- uncertainties in the acceptance due to the modelling by PYTHIA were accounted for by taking half of the change attributable to the reweighting as a systematic uncertainty; for most points the effect was small.

The background from photoproduction events at low Q^2 was found to be negligible. Other sources of systematic uncertainty were found to be negligible and were ignored [9]: these included the modelling of the ΔR cut, the track momentum cut, the cut on $E - p_Z$, the $Z_{\rm vtx}$ cut, the cut on the electromagnetic fraction of the photon shower, and a variation of 5% on the LL fraction. These were found to generate systematic effects of at most 1-2% apart from a 2.5% effect in the highest-x bin.

The major uncertainties were treated as symmetric and added in quadrature. The common uncertainty of 1.8% on the luminosity measurement was not included in the tables and figures.

8 Results

Differential cross sections in DIS for the production of an isolated photon and at least one additional jet, $ep \to e'\gamma + \text{jet}$, were measured in the kinematic region defined by $10 < Q^2 < 350\,\text{GeV}^2$, $E'_e > 10\,\text{GeV}$, $\theta_e > 140^\circ$, $-0.7 < \eta^\gamma < 0.9$, $4 < E_T^\gamma < 15\,\text{GeV}$, $E_T^{\text{jet}} > 2.5$ GeV and $-1.5 < \eta^{\text{jet}} < 1.8$ in the laboratory frame. The jets were formed according to the k_T-clustering algorithm with the R parameter set to 1.0, and photon isolation was imposed such that at least 90% of the energy of the jet-like object containing the photon belongs to the photon. No track with momentum greater than 250 MeV was allowed within a cone around the photon of radius 0.2 in η, ϕ.

The differential cross sections as functions of Q^2, x, E_T^γ, η^γ, E_T^{jet} and η^{jet} are shown in Fig. 3 and given in Tables 1–6. As expected, the cross section decreases with increasing Q^2, x, E_T^γ, and E_T^{jet}. The modest dependence of the cross section on η^γ and η^{jet} can be attributed to the LL contribution. The predictions for the sum of the expected LL contribution from Djangoh and a factor of 1.6 times the expected QQ contribution from Pythia agree well with the measurements, and this model therefore provides a good description of the process.

The theoretical predictions described in Section 4 are compared to the measurements in Fig. 4. The predictions from GKS [39] describe the shape of all the distributions reasonably well, but the rise seen at low Q^2 and at low x is underestimated. The cross section as a function of η^γ and η^{jet} is underestimated by about 20%. This was also observed in the earlier inclusive photon measurement [9]. The theoretical uncertainties are indicated by the width of the shaded area. The calculations of BLZ [40] also describe the shape of the data reasonably well, but the predicted overall rate is too high by about 20%.

9 Conclusions

The production of isolated photons accompanied by jets has been measured in deep inelastic scattering with the ZEUS detector at HERA using an integrated luminosity of $326\,\text{pb}^{-1}$. The present results improve on earlier ZEUS results [7] which were made with an integrated luminosity of 121 pb^{-1} in a more restricted kinematic region. Differential cross sections as functions of several variables are presented within the kinematic region defined by: $10 < Q^2 < 350\,\text{GeV}^2$, $E'_e > 10\,\text{GeV}$, $\theta_e > 140^\circ$, $-0.7 < \eta^\gamma < 0.9$, $4 < E_T^\gamma < 15\,\text{GeV}$, $E_T^{\text{jet}} > 2.5$ GeV and $-1.5 < \eta^{\text{jet}} < 1.8$ in the laboratory frame. The order $\alpha^3\alpha_s$ predictions of Gehrmann-de Ridder *et al.* reproduce the shapes of all the measured experimental distributions reasonably well, as do the predictions of Baranov *et al.* However neither calculation gives a correct normalisation. The results presented here can be used to make further improvements in the QCD calculations.

Acknowledgements

We appreciate the contributions to the construction and maintenance of the ZEUS detector of many people who are not listed as authors. The HERA machine group and the DESY computing staff are especially acknowledged for their success in providing excellent operation of the collider and the data-analysis environment. We thank the DESY directorate for their strong support and encouragement. We also thank H. Spiesberger and N. Zotov for providing theoretical results.

References

[1] E. Anassontzis et al., Z. Phys. C 13 (1982) 277;
WA70 Collaboration, M. Bonesini et al., Z. Phys. C 38 (1988) 371;
E706 Collaboration, G. Alverson et al., Phys. Rev. D 48 (1993) 5;
CDF Collaboration, F. Abe et al., Phys. Rev. Lett. 73 (1994) 2662;
CDF Collaboration, D. Acosta et al., Phys. Rev. Lett. 95 (2005) 022003;
DØ Collaboration, B. Abbott et al., Phys. Rev. Lett. 84 (2000) 2786;
DØ Collaboration, V.M. Abazov et al., Phys. Lett. B 639 (2006) 151.

[2] ZEUS Collaboration, J. Breitweg et al., Phys. Lett. B 413 (1997) 201.

[3] ZEUS Collaboration, J. Breitweg et al., Phys. Lett. B 472 (2000) 175.

[4] ZEUS Collaboration, S. Chekanov et al., Phys. Lett. B 511 (2001) 19.

[5] ZEUS Collaboration, S Chekanov et al., Eur. Phys. J. C 49 (2007) 511.

[6] H1 Collaboration, A. Aktas et al., Eur. Phys. J. C 38 (2004) 437.

[7] ZEUS Collaboration, S. Chekanov et al., Phys. Lett. B 595 (2004) 86.

[8] H1 Collaboration, F.D. Aaron et al., Eur. Phys. J. C 54 (2008) 371.

[9] ZEUS Collaboration, S. Chekanov et al., Phys. Lett. B 687 (2010) 16.

[10] A.D. Martin et al., Eur. Phys. J. C 39 (2005) 155.

[11] A. Gehrmann-De Ridder, G. Kramer and H. Spiesberger,Nucl. Phys. B 578 (2000) 326.

[12] A. Gehrmann-De Ridder, T. Gehrmann and E. Poulsen, Phys. Rev. Lett. 96 (2006) 132002.

[13] A. Gehrmann-De Ridder, T. Gehrmann and E. Poulsen, Eur. Phys. J. C 47 (2006) 395.

[14] S. Baranov, A. Lipatov and N. Zotov, Phys. Rev. D 81 (2010) 094034.

[15] ZEUS Collaboration, U. Holm (ed.), *The ZEUS Detector. Status Report* (unpublished), DESY (1993),
available on `http://www-zeus.desy.de/bluebook/bluebook.html`.

[16] N. Harnew et al., Nucl. Inst. Meth. A 279 (1989) 290;
B. Foster et al., Nucl. Phys. Proc. Suppl. B 32 (1993) 181;
B. Foster et al., Nucl. Inst. Meth. A 338 (1994) 254.

[17] A. Polini et al., Nucl. Inst. Meth. A 581 (2007) 656.

[18] M. Derrick et al., Nucl. Inst. Meth. A 309 (1991) 77;
A. Andresen et al., Nucl. Inst. Meth. A 309 (1991) 101;
A. Caldwell et al., Nucl. Inst. Meth. A 321 (1992) 356;
A. Bernstein et al., Nucl. Inst. Meth. A 336 (1993) 23.

[19] J. Andruszków et al., Preprint DESY-92-066, DESY, 1992;
ZEUS Collaboration, M. Derrick et al., Z. Phys. C 63 (1994) 391;
J. Andruszków et al., Acta Phys. Pol. B 32 (2001) 2025.

[20] M. Heilbich et al., Nucl. Inst. Meth. A 565 (2006) 572.

[21] W.H. Smith, K. Tokushuku and L.W. Wiggers, *Proc. Computing in High-Energy Physics (CHEP), Annecy, France, Sept. 1992*, C. Verkerk and W. Wojcik (eds.), p. 222. CERN, Geneva, Switzerland (1992). Also in preprint DESY 92-150B.

[22] P. Allfrey, Nucl. Inst. Meth. A 580 (2007) 1257.

[23] H. Abramowicz, A. Caldwell and R. Sinkus, Nucl. Inst. Meth. A 365 (1995) 508;
R. Sinkus and T. Voss, Nucl. Inst. Meth. A 391 (1997) 360.

[24] ZEUS Collaboration, M. Derrick et al., Phys. Lett. B 303 (1993) 183.

[25] ZEUS Collaboration, J. Breitweg et al., Eur. Phys. J. C 1 (1998) 81;
ZEUS Collaboration, J. Breitweg et al., Eur. Phys. J. C 6 (1999) 43;
G.M. Briskin, Ph.D. Thesis, Tel Aviv University (1998) DESY-THESIS-1998-036.

[26] S. Catani et al., Nucl. Phys. B 406 (1993) 187.

[27] S.D. Ellis and D.E. Soper, Phys. Rev. D 48 (1993) 3160.

[28] H1 and ZEUS Collaborations, F. D. Aaron et al., JHEP 01 (2010) 109.

[29] L. Bourhis, M. Fontannaz and J.Ph. Guillet, Eur. Phys. J. C 2 (1998) 529.

[30] T. Sjöstrand et al., JHEP 0605 (2006) 26.

[31] K. Charchuła, G.A. Schuler and H. Spiesberger, Comp. Phys. Comm. 81 (1994) 381.

[32] A. Kwiatkowski, H. Spiesberger and H.-J. Möhring, Comp. Phys. Comm. 69 (1992) 155.

[33] L. Lönnblad, Comp. Phys. Comm. 71 (1992) 15.

[34] T. Sjöstrand, Comp. Phys. Comm. 39 (1986) 347.

[35] B. Andersson et al., Phys. Rev. 97 (1983) 31.

[36] R. Brun et al., GEANT3, Technical Report CERN-DD/EE/84-1, CERN (1987).

[37] M. Forrest, Ph.D. Thesis, University of Glasgow (2010) (unpublished), http://theses.gla.ac.uk/1761/ .

[38] ZEUS Collaboration, S. Chekanov et al., Eur. Phys. J. C 62 (2009) 625.

[39] H. Spiesberger, private communication.

[40] N. Zotov, private communication.

Q^2 range (GeV^2)	$\frac{d\sigma}{dQ^2}$ ($\mathrm{pb\,GeV}^{-2}$)
10 – 20	$0.298 \pm 0.024\,(\mathrm{stat.}) \pm 0.019\,(\mathrm{sys.})$
20 – 40	$0.129 \pm 0.012\,(\mathrm{stat.}) \pm 0.009\,(\mathrm{sys.})$
40 – 80	$0.049 \pm 0.005\,(\mathrm{stat.}) \pm 0.004\,(\mathrm{sys.})$
80 – 150	$0.0224 \pm 0.0023\,(\mathrm{stat.}) \pm 0.0011\,(\mathrm{sys.})$
150 – 350	$0.0037 \pm 0.0007\,(\mathrm{stat.}) \pm 0.0002\,(\mathrm{sys.})$

Table 1: Measured differential cross-section $\frac{d\sigma}{dQ^2}$. The quoted systematic uncertainty includes all the components added in quadrature.

x range	$\frac{d\sigma}{dx}$ (pb)
0.0002 – 0.001	$4869 \pm 334\,(\mathrm{stat.}) \pm 312\,(\mathrm{sys.})$
0.001 – 0.003	$1811 \pm 139\,(\mathrm{stat.}) \pm 104\,(\mathrm{sys.})$
0.003 – 0.01	$278 \pm 31\,(\mathrm{stat.}) \pm 13\,(\mathrm{sys.})$
0.01 – 0.02	$25 \pm 7\,(\mathrm{stat.}) \pm 3\,(\mathrm{sys.})$

Table 2: Measured differential cross-section $\frac{d\sigma}{dx}$. Details as in Table 1.

E_T^γ range (GeV)	$\frac{d\sigma}{dE_T^\gamma}$ ($\mathrm{pb\,GeV}^{-1}$)
4 – 6	$2.38 \pm 0.18\,(\mathrm{stat.}) \pm 0.13\,(\mathrm{sys.})$
6 – 8	$1.28 \pm 0.10\,(\mathrm{stat.}) \pm 0.06\,(\mathrm{sys.})$
8 – 10	$0.62 \pm 0.08\,(\mathrm{stat.}) \pm 0.04\,(\mathrm{sys.})$
10 – 15	$0.26 \pm 0.03\,(\mathrm{stat.}) \pm 0.02\,(\mathrm{sys.})$

Table 3: Measured differential cross-section $\frac{d\sigma}{dE_T^\gamma}$. Details as in Table 1.

η^γ range	$\frac{d\sigma}{d\eta^\gamma}$ (pb)
–0.7 – –0.3	$7.6 \pm 0.6\,(\mathrm{stat.}) \pm 0.5\,(\mathrm{sys.})$
–0.3 – 0.1	$6.7 \pm 0.5\,(\mathrm{stat.}) \pm 0.3\,(\mathrm{sys.})$
0.1 – 0.5	$5.8 \pm 0.6\,(\mathrm{stat.}) \pm 0.3\,(\mathrm{sys.})$
0.5 – 0.9	$5.2 \pm 0.5\,(\mathrm{stat.}) \pm 0.4\,(\mathrm{sys.})$

Table 4: Measured differential cross-section $\frac{d\sigma}{d\eta^\gamma}$. Details as in Table 1.

$E_T^{\rm jet}$ range (GeV)	$\frac{d\sigma}{dE_T^{\rm jet}}$ (pb GeV^{-1})
2.5 – 4	1.40 ± 0.16 (stat.) ± 0.08 (sys.)
4 – 6	1.19 ± 0.11 (stat.) ± 0.10 (sys.)
6 – 8	1.01 ± 0.10 (stat.) ± 0.07 (sys.)
8 – 10	0.74 ± 0.07 (stat.) ± 0.05 (sys.)
10 – 15	0.32 ± 0.03 (stat.) ± 0.02 (sys.)
15 – 35	0.031 ± 0.006 (stat.) ± 0.003 (sys.)

Table 5: Measured differential cross-section $\frac{d\sigma}{dE_T^{\rm jet}}$. Details as in Table 1.

$\eta^{\rm jet}$ range	$\frac{d\sigma}{d\eta^{\rm jet}}$ (pb)
–1.5 – –0.7	1.53 ± 0.17 (stat.) ± 0.15 (sys.)
–0.7 – 0.1	2.84 ± 0.25 (stat.) ± 0.19 (sys.)
0.1 – 0.9	3.91 ± 0.33 (stat.) ± 0.14 (sys.)
0.9 – 1.8	3.57 ± 0.29 (stat.) ± 0.22 (sys.)

Table 6: Measured differential cross-section $\frac{d\sigma}{d\eta^{\rm jet}}$. Details as in Table 1.

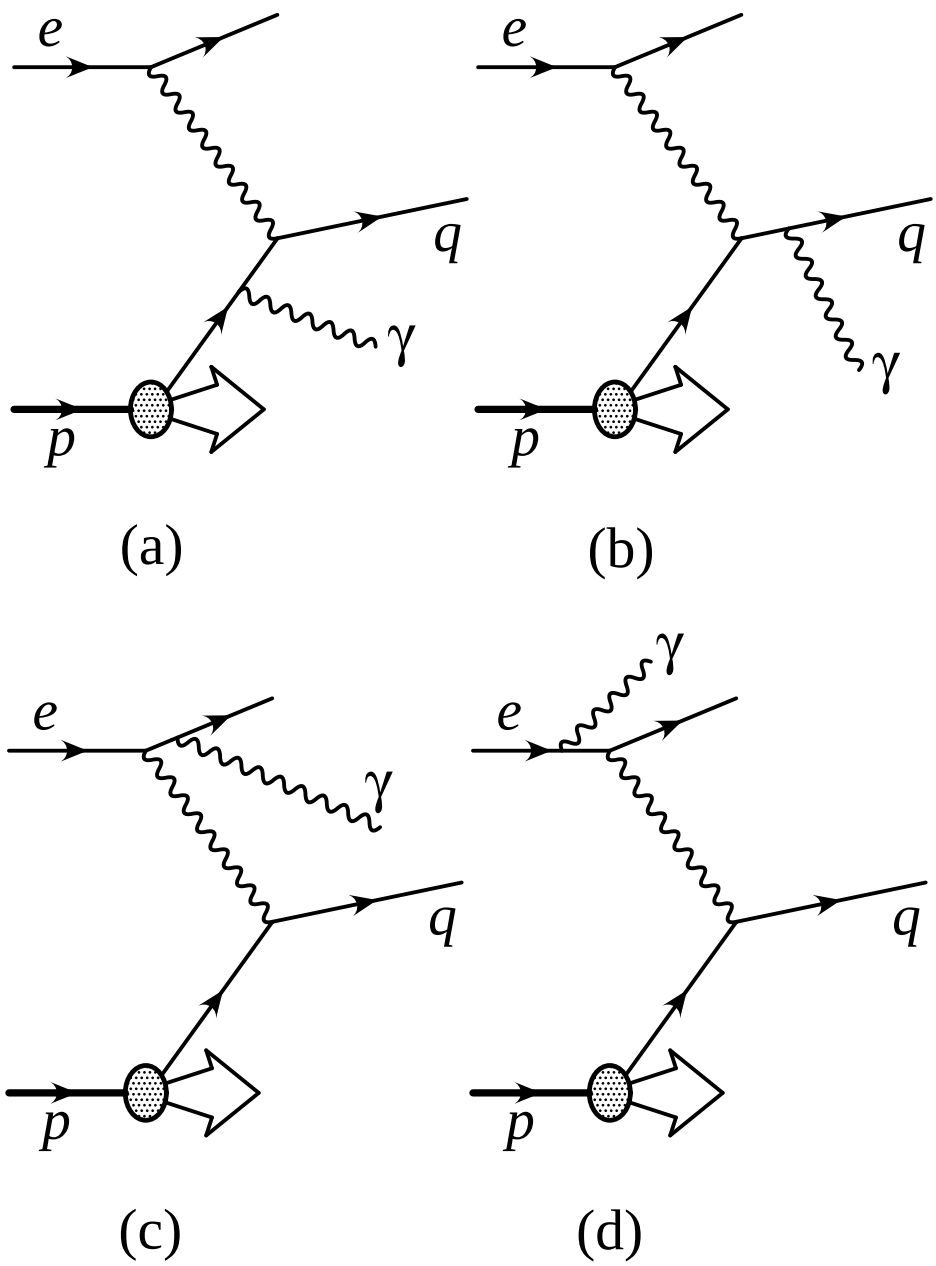

Figure 1: Lowest-order tree-level diagrams for isolated photon production in *ep* scattering. (a) - (b): quark radiative diagrams; (c) - (d): lepton radiative diagrams.

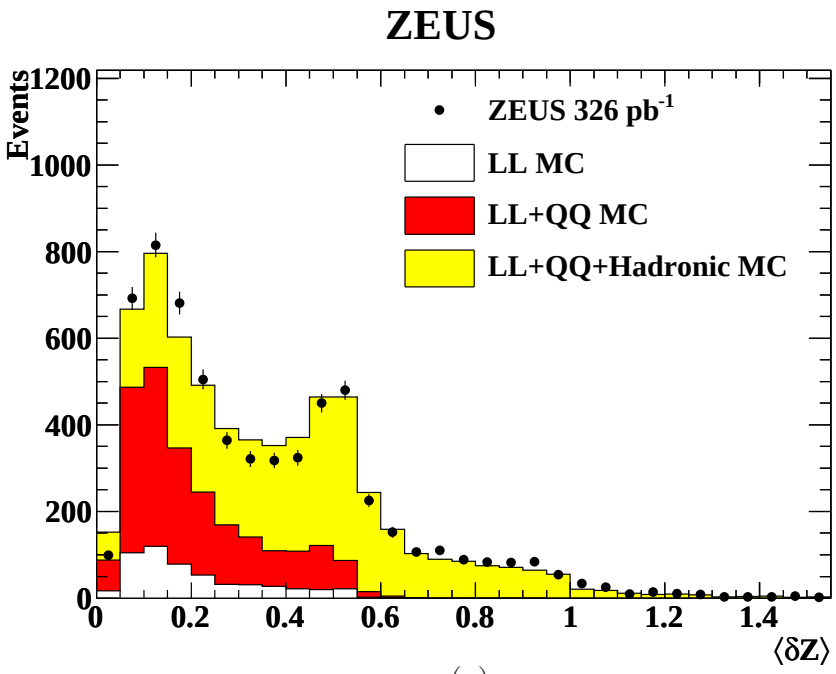

(a)

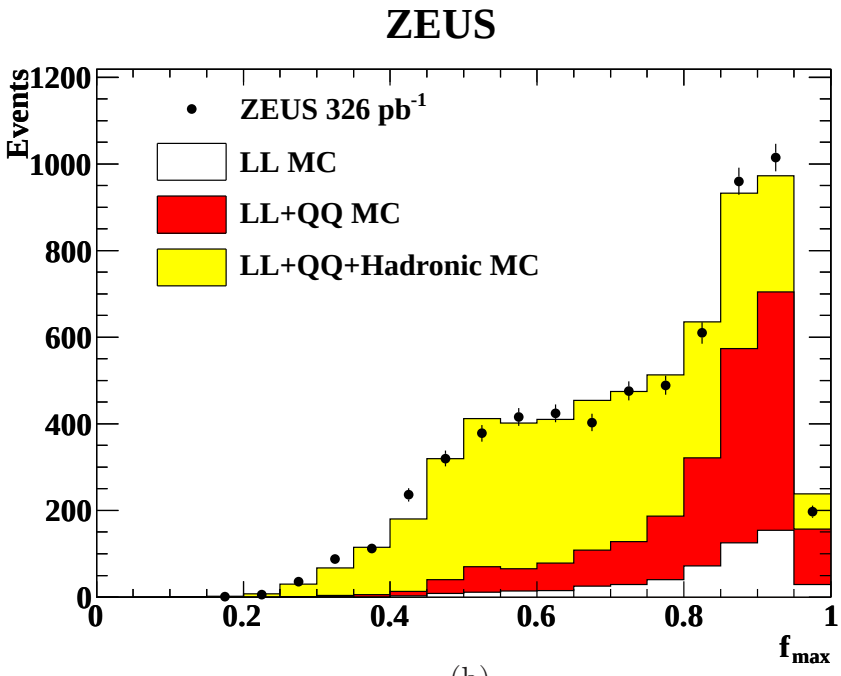

(b)

Figure 2: Distribution of (a) $\langle \delta Z \rangle$, (b) $f_{\max}$. The error bars represent the statistical uncertainties. The light shaded histogram shows a fit to the data of three components with fixed shapes as described in the text. The dark shaded histogram represents the QQ component of the fit, and the white histogram the LL component.

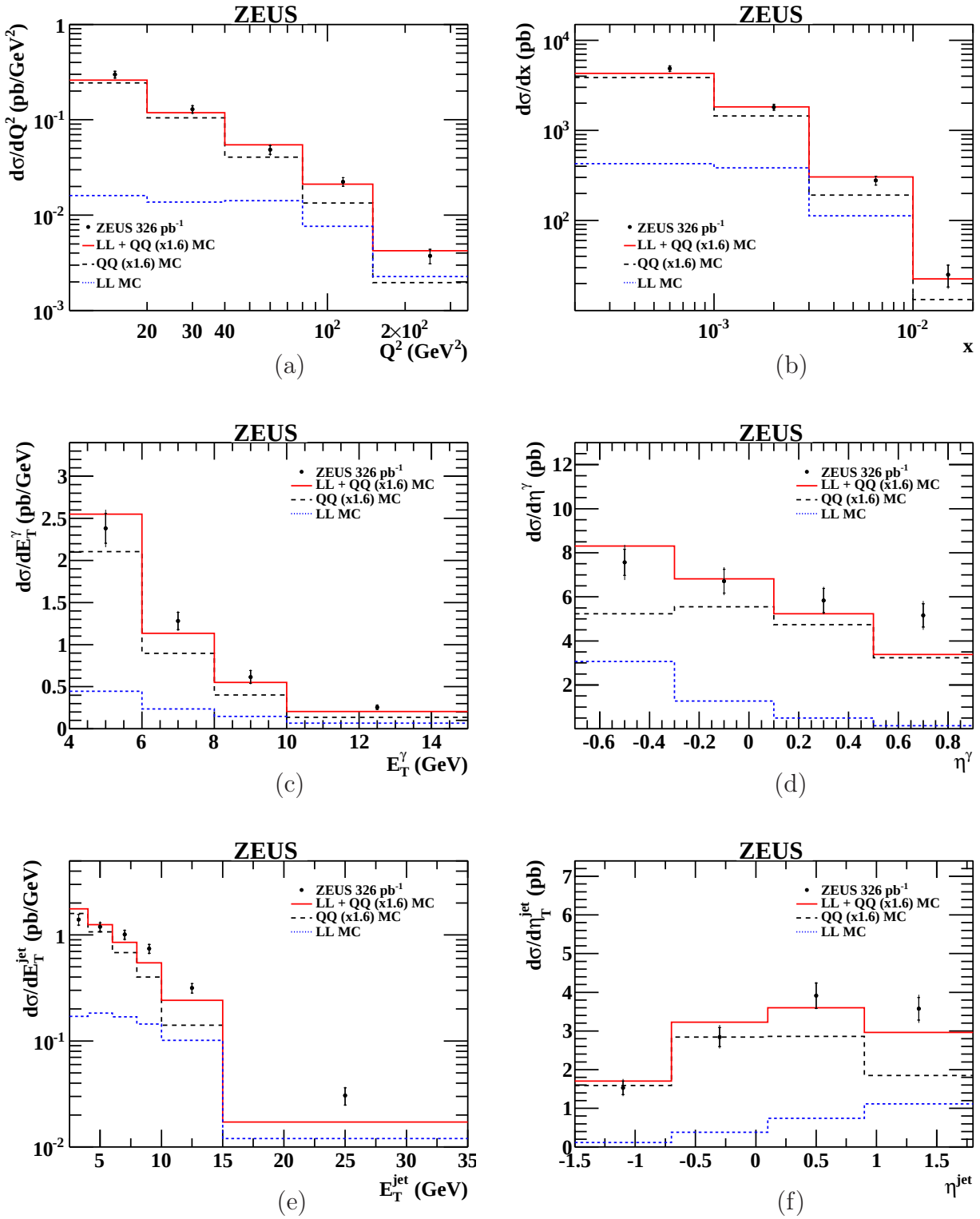

Figure 3: Isolated photon differential cross sections in (a) Q^2, (b) x, (c) E_T^γ, (d) η^γ, (e) $E_T^{\rm jet}$, and (f) $\eta^{\rm jet}$. The inner and outer error bars show, respectively, the statistical uncertainty and the statistical and systematic uncertainties added in quadrature. The solid histograms are the reweighted Monte Carlo predictions from the sum of QQ photons from PYTHIA normalised by a factor 1.6 plus DJANGOH LL photons. The dashed (dotted) lines show the QQ (LL) contributions.

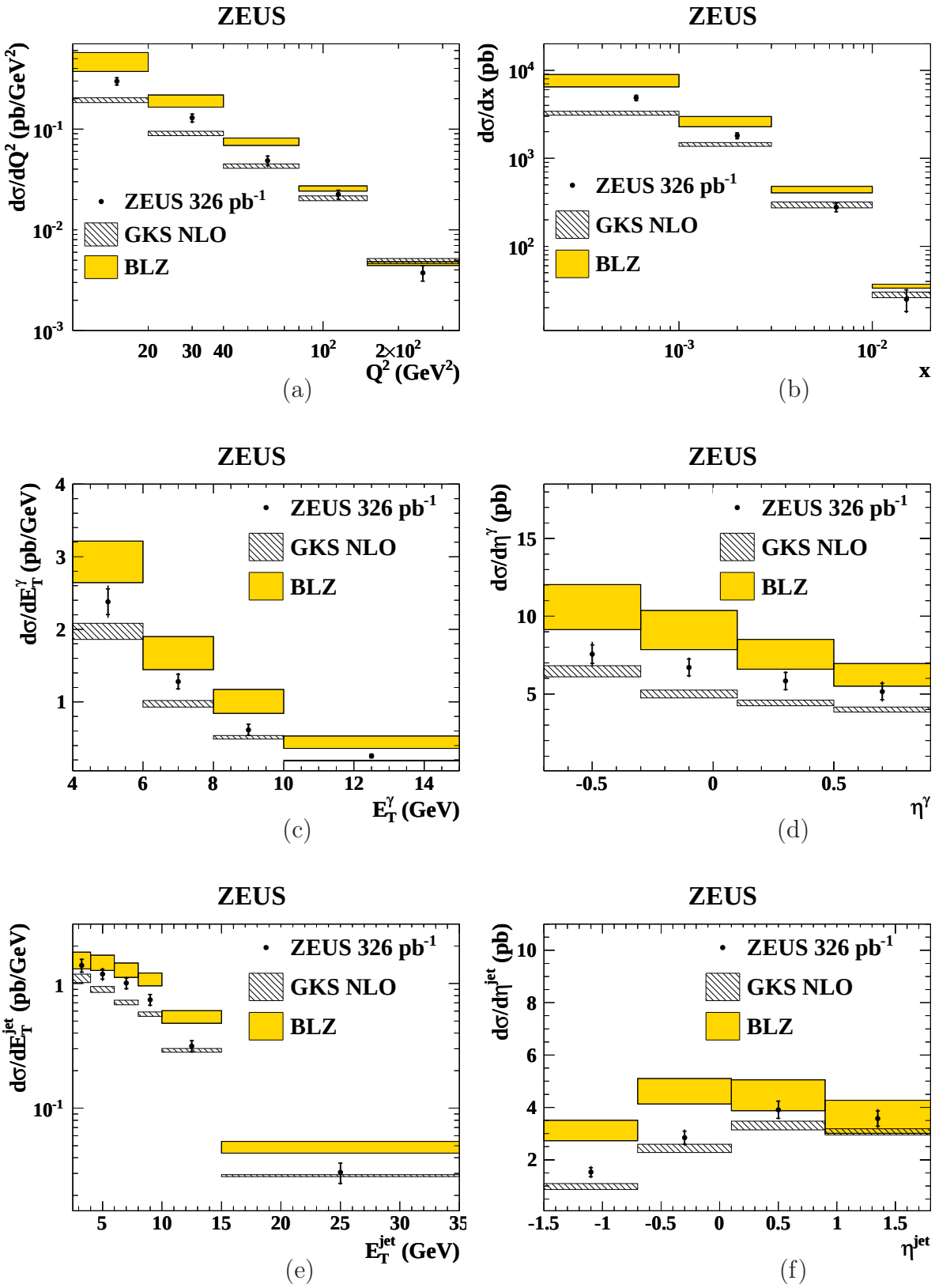

Figure 4: Data points as shown in Fig. 3. Theoretical predictions from Gehrmann-De Ridder *et al.* (GKS) [39] and Baranov *et al.* (BLZ) [40] are shown, with associated uncertainties indicated by the shaded bands.